THE IMPORTANCE OF SMALL SCALE PROCESSES IN GLOBAL MHD SIMULATIONS: SOME NUMERICAL EXPERIMENTS

Joachim Raeder, Jean Berchem, and Maha Ashour-Abdalla
Institute of Geophysics and Planetary Physics
University of California, Los Angeles, Ca 90095-1567

ABSTRACT

We have used our global MHD model to assess the importance of small scale processes for magnetospheric dynamics. The comparison of two simulation runs, one with, and one without anomalous resistivity, and with otherwise identical parameters, shows that a substorm only develops when anomalous resistivity is present. A similar comparison of a simulation run with a self-consistent ionospheric conductance model and a run in which the ionospheric conductance was increased, shows that increased ionospheric conductance can likewise prevent the occurrence of a substorm. We conclude that the proper parameterization of these small scale processes is important for global modeling of the magnetosphere. Our results also show that substorm models must account for localized processes, like the occurrence of anomalous resistivity, as well as for the response of the ionosphere.

I. INTRODUCTION

Interactions between the solar wind and magnetospheric plasmas are dominated by collisionless processes. Because the processes are collisionless, these plasmas and their interactions should in general be characterized by the Vlasov-Maxwell equations. However, in many instances, especially when the spatial scales under consideration are large compared to the local ion gyroradius and the temporal scales exceed the ion gyroperiod, the much cruder MHD description suffices. Indeed, many theoretical studies, experimental analyses, and numerical simulations are based on the relatively simple MHD description.

The global modeling of the Earth's magnetosphere and its interaction with the solar wind is an example of the successful application of the MHD approximation. Many such models have been developed over the past two decades [1-5], and these models have successfully reproduced many of the gross features of the solar wind-magnetosphere interaction and the associated large scale processes. More recently, direct comparisons between our model and observations [6] have shown that global MHD models, when driven by measured solar wind conditions, are capable of predicting those observations in the magnetosphere.

A closer look at the intricate structure of global MHD models shows that

they are in fact not really ideal MHD models, and that they work only because small scale processes that cause a deviation from ideal MHD are implicitly or explicitly included in the models. Many of the deviations from ideal MHD arise from numerical effects; in fact there is no numerical scheme that could solve the ideal (i.e., hyperbolic) MHD equations without introducing numerical diffusion, dispersion, or both. However, these effects, if well understood and controlled, are not necessarily harmful to the solutions, and may even be an essential ingredient.

One example is Earth's bow shock. It can only exist because kinetic processes provide enough diffusion for the shock to increase the plasma entropy sufficiently. Therefore, in the shock transition region, the plasma cannot be described as an ideal MHD fluid. However, when the MHD equations are supplemented with proper diffusion terms, they contain enough of the shock physics to describe the bow shock on the large scale.

Similarly, any numerical scheme for solving a shock transition (or any type of discontinuity) must also employ a certain amount of diffusion. If the scheme does not generate enough diffusion in the shock transition region, other (unavoidable) numerical effects, like grid aliasing and wave dispersion, will dominate. These will effectively destroy the physical solution by creating large amplitude, high frequency waves in the vicinity of the discontinuity[1]. As a consequence, discontinuities can only be obtained in simulations by effectively altering the MHD equations and adding diffusive terms. This can be done in different ways, either by using difference equations that have diffusive error terms (for example the upwind scheme, or the Lax-Wendroff schemes [8]), or by adding diffusive terms explicitly. In fact, the major difference between simulation models is the way in which the diffusion terms are handled. The "classical" schemes, for example the Lax-Wendroff scheme, add diffusion globally, i.e., everywhere in the simulation domain. The obvious disadvantage is that diffusion is added to regions where it is not desirable. On the other hand, "modern" schemes, for example hybridized schemes like FCT (Flux Corrected Transport) and TVD (Total Variance Diminishing) schemes [9], are very sensitive to gradients in the solution, and add diffusion only locally, where steep gradients would otherwise lead to severe numerical aliasing and dispersion. In regions of smooth flow, "modern" schemes attempt to minimize diffusion. Thus, the "modern" schemes closely mimic nature by creating diffusion just within the shock transition layer (which is typically only 1-2 gridpoints thick), albeit for very different reasons. The actual amount of numerical diffusion in the transition layer is of little concern if the numerical scheme is conservative, i.e., based on the conservative MHD equations, because conservative finite differences always exactly fulfill the Rankine-Hugoniot jump conditions.

---

[1] A prominent example is the Leap-Frog scheme which has no numerical diffusion, but is very dispersive. Because of the numerical dispersion it is useless for computations that include discontinuities; an example can be found in [7].

Besides shock dissipation there is a large number of other small scale processes that have the potential of affecting the large scale interaction of Earth's magnetosphere with the solar wind. In this paper we will consider two of these processes. First, we will show the effect of anomalous resistivity on the tail dynamics. Although numerical resistivity is present in our model and allows for magnetic reconnection, the addition of a nonlinear resistivity term to Ohm's Law substantially alters the tail dynamics and leads to more realistic results. Second, we will examine the effects of different levels of ionospheric conductance on magnetospheric dynamics. The ionosphere is implemented as a boundary condition for the MHD domain; and the dominating processes, such as field aligned potential drops, electron acceleration, and ionization are inherently kinetic and must be properly parameterized.

In the following, we will first briefly describe our model. We will then compare three different simulation runs, one reference run with anomalous resistivity and a fully implemented ionosphere, one in which the anomalous resistivity is switched off, and one in which the ionospheric Hall and Pedersen conductances are set to artificially high values. We will then discuss these results with respect to the proper parameterization of these small scale processes.

II. THE MODEL

For this study we use a global MHD code which includes an ionospheric model for the closure of field aligned currents. In order to accommodate the large simulation volume with a 400 R_E tail and long simulation times the simulation code was parallelized for running on MIMD (Multiple Instruction - Multiple Data) machines by using a domain decomposition technique. The model solves the ideal MHD equations (modified as described below) for the magnetosphere and a potential equation for the ionosphere. As we discussed in the introduction, numerical effects, like diffusion, viscosity, and resistivity, are necessarily introduced by the numerical methods. These permit viscous interactions and also magnetic field reconnection to a limited extent. The only explicit diffusive term is the anomalous resistivity that is included in Ohm's Law.

The magnetospheric (MHD) part of the model is solved using a finite difference method which is conservative for the gas-dynamic part of the MHD equations:

$$\frac{\partial \rho}{\partial t} = -\underline{\nabla} \cdot (\rho \underline{\mathbf{v}})$$

$$\frac{\partial \rho \underline{\mathbf{v}}}{\partial t} = -\underline{\nabla} \cdot (\rho \underline{\mathbf{v}}\underline{\mathbf{v}} + p\underline{\underline{\mathbf{I}}}) + \underline{\mathbf{j}} \times \underline{\mathbf{B}}$$

$$\frac{\partial e}{\partial t} = -\underline{\nabla} \cdot (\{e + p\}\underline{\mathbf{v}}) + \underline{\mathbf{j}} \cdot \underline{\mathbf{E}}$$

$$\frac{\partial \underline{\mathbf{B}}}{\partial t} = -\underline{\nabla} \times \underline{\mathbf{E}}$$

$$\underline{\nabla} \cdot \underline{\mathbf{B}} = 0$$

$$\underline{\mathbf{E}} = -\underline{\mathbf{v}} \times \underline{\mathbf{B}} + \eta \underline{\mathbf{j}}$$

$$\underline{\mathbf{j}} = \underline{\nabla} \times \underline{\mathbf{B}}$$

$$e = \frac{1}{2}\rho v^2 + \frac{p}{\gamma - 1}$$

where the symbols have their usual meaning. The $\underline{\mathbf{j}} \times \underline{\mathbf{B}}$ and $\underline{\mathbf{E}} \cdot \underline{\mathbf{j}}$ terms are treated as source terms because the very low plasma β and the large magnetic field gradients near the Earth do not allow the use of the full conservative form of the MHD equations. The model of the anomalous resistivity is given by:

$$\eta = \alpha {j_1}^2 \quad , \quad j_1 = \begin{cases} j_2 & \text{if } j_2 \geq \delta \\ 0 & \text{else} \end{cases} \quad , \quad j_2 = \frac{|j|\Delta}{|B| + \epsilon}$$

where j is the local current density, B the local magnetic field, Δ is the gridspacing, and ϵ is a very small number introduced to avoid dividing by zero. j_2 is the normalized current density ($0 \leq j_2 \leq 1$) that is used as a switch for the resistivity. In places where the resistivity is switched on it becomes proportional to the square of the local current density. Similar resistivity models have been used in the past to model the kinetic effects that lead to anomalous resistivity [10, 11]. The parameters α and δ determine the value of the resistivity and the current density threshold that must be reached for the resistivity to be switched on. These parameters are choosen such that the resistivity η is nonzero only at very few gridpoints in strong current sheets.

The numerical grid is rectangular and nonuniform with the highest spatial resolution near Earth (about 0.5 R_E). It extends 30 R_E in the sunward direction, 400 R_E in the tailward direction and 70 R_E in the Y and Z directions. The gas-dynamic part of the equations is spatially differenced by using a technique in which fourth order fluxes are hybridized with first order (Rusanov) fluxes [9,12]. The magnetic induction equation is treated somewhat differently [13] in order to conserve $\nabla \cdot \mathbf{B} = 0$ exactly. The time stepping scheme for all variables consists of a low order predictor with a time centered corrector, which is second order accurate in time. The outer boundary conditions are fixed at the given solar wind values on the upstream side. At the other boundaries we apply open, i.e., zero normal derivative, boundary conditions.

The inner boundary, where the MHD quantities are connected to the ionosphere, is taken to be a shell of radius 3.7 R_E centered of Earth. The choice of this radius is a compromise and necessitated by numerical considerations, such as extraneously high Alfven speeds and very large magnetic field gradients closer to the Earth. However, this choice allows for the proper mapping of all relevant field aligned current (FAC) systems. Inside this shell we do not solve the MHD equations, but assume a static dipole field. The important physical processes within the shell are the flow of field aligned currents and the closure of these currents in the ionosphere. At each time step we map the magnetospheric FACs from the 3.7 R_E shell onto the polar cap using a static dipole field. We then use the FACs as input for the ionospheric potential equation:

$$\underline{\nabla} \cdot \underline{\underline{\mathbf{\Sigma}}} \cdot \underline{\nabla} \Phi = -j_{\parallel} \sin I$$

which is solved on the surface of a sphere with a radius of 1 R_E. Here Φ denotes the ionospheric potential, $\underline{\underline{\mathbf{\Sigma}}}$ is the tensor of the ionospheric conductance, $j_{\parallel}$ is the

mapped FAC with the downward current considered positive and corrected for flux tube convergence, and I is the inclination of the dipole field at the ionosphere. The boundary condition $\Phi = 0$ is applied at the equator. For the ionospheric Hall and Pedersen conductances, Σ_H and Σ_P, which enter the conductance tensor $\underline{\underline{\boldsymbol{\Sigma}}}$ [14], three ionization sources are taken into account. First, for the solar EUV ionization we use an empirical model [15] that depends solely on the solar 10.7 cm flux ($F_{10.7}$) and the solar zenith angle (χ):

$$\Sigma_H = (F_{10.7})^{0.53}(0.81\cos\chi + 0.54\cos^{1/2}\chi)$$
$$\Sigma_P = (F_{10.7})^{0.49}(0.34\cos\chi + 0.93\cos^{1/2}\chi)$$

Second, we compute the mean energy E_0 and energy flux F_E of precipitating electrons that are accelerated by a parallel potential drop $\Delta\Phi$ in regions of upward field aligned currents [16,17]:

$$F_E = \Delta\Phi_\parallel |j_\parallel| \qquad , \qquad E_0 = e\Delta\Phi_\parallel$$

$$\Delta\Phi = K\max(0, -j_\parallel) \qquad , \qquad K = \frac{e^2 n_e}{\sqrt{2\pi m_e k T_e}}$$

Third, diffuse electron precipitation is modeled by assuming complete pitch angle scattering of electrons at 3.7 R_E[18]:

$$F_E = n_e(kT_e/2\pi m_e)^{\frac{1}{2}} \qquad , \qquad E_0 = kT_e$$

Here, n_e, T_e, and m_e are the electron density, temperature, and mass, respectively, taken at the 3.7 R_E shell. The conductances are then computed from the electron precipitation parameters using the empirical relations [19]:

$$\Sigma_P = [40E_0/(16 + E_0^2)]F_E^{1/2} \qquad , \qquad \Sigma_H = 0.45E_0^{5/8}\Sigma_P$$

Using the mapped FACs and ionospheric conductances the potential equation is solved, and the the ionospheric potential is mapped to the 3.7 R_E shell where it is used as a boundary condition for the magnetospheric flow by taking $\underline{\mathbf{v}} = (-\underline{\nabla}\Phi)\times\underline{\mathbf{B}}/B^2$.

The initial conditions for the magnetic field are constructed from the superposition of Earth's dipole over a mirror dipole, such that B_x vanishes at x = 16 R_E. Sunward of the plane of symmetry at 16 R_E the field is replaced by the initial solar wind field. This procedure ensures a divergence-free transition from the constant solar wind field to Earth's dipole field. The simulation box is initially filled with tenuous (0.1 cm^{-3}) and cold (5000^0 K) plasma of zero velocity. The solar wind flow is switched on at the sunward boundary at time t=0.

III. RESULTS

In order to assess the effects of the parameterized small scale processes in a global simulation we compare three simulation runs with identical solar wind conditions. The solar wind density, temperature and velocity are held constant at average values (7.3 cm^{-3}, 5×10^4 K and 420 km/s). The IMF is due south for the first 60 minutes (B_z = -5 nT), then due north for the next 60 minutes (B_z = 5 nT). After that, the IMF goes southward again (B_z = -5 nT) and remains so until the end of the runs. The IMF B_x and B_y components are assumed to be zero.

During the first 60 minutes the magnetosphere develops from its unphysical initial state. The following 60 minutes of northward IMF see the magnetosphere evolve into a quiet configuration. This does not imply that the simulated magnetosphere reaches a steady state. In fact, an X-line that developed during the preceding southward interval remains intact in the center of the tail while the tail flanks are replaced by a broad and growing boundary layer. Details of the tail morphology during times of strong northward IMF have been reported in [5]. After the IMF turns southward again at t = 120 min, one would expect that a substorm would develop. As we will show below, whether or not a substorm occurs in the simulation depends critically on the parameterization of the anomalous resistivity and the ionospheric conductances.

1.) *Self-consistent ionosphere and anomalous resistivity*

In this reference run we have included the self-consistent ionosphere model and the anomalous resistivity terms that we described in section II. The parameters for the resistivity model were set to δ = 0.5 and α = 0.02. Figs. 1a through 1d show a time sequence of the evolution of the magnetic field in the noon--midnight meridional plane. At time t = 125 min (Fig. 1a) the southward IMF just reaches the subsolar magnetopause. There are no changes apparent in the tail from the previous northward IMF period. Note that the tail neutral line only exists in the very center of the tail at this time [5]. Ten minutes later (Fig. 1b), reconnection has begun at the subsolar magnetopause between magnetospheric field lines and magnetosheath field lines. In the tail, the field between about -10 R_E and -25 R_E has become more dipolar and the neutral line has moved a few R_E tailward. After another ten minutes (Fig. 1c), the tail neutral line has moved to about -35 R_E. Earthward, the closed field line region has become stretched, which may be interpreted as a substorm growth phase. Within the next 5 minutes, tearing occurs in the closed field line region and a plasmoid is formed (Fig. 1d).

Clearly, these results show some proximity to typically observed substorm features, in particular the formation and ejection of a plasmoid [20]. Also, the ionospheric parameters (not shown here) are in basic agreement with substorm observations. In particular, we see the development of a substorm current system and a westward travelling surge.

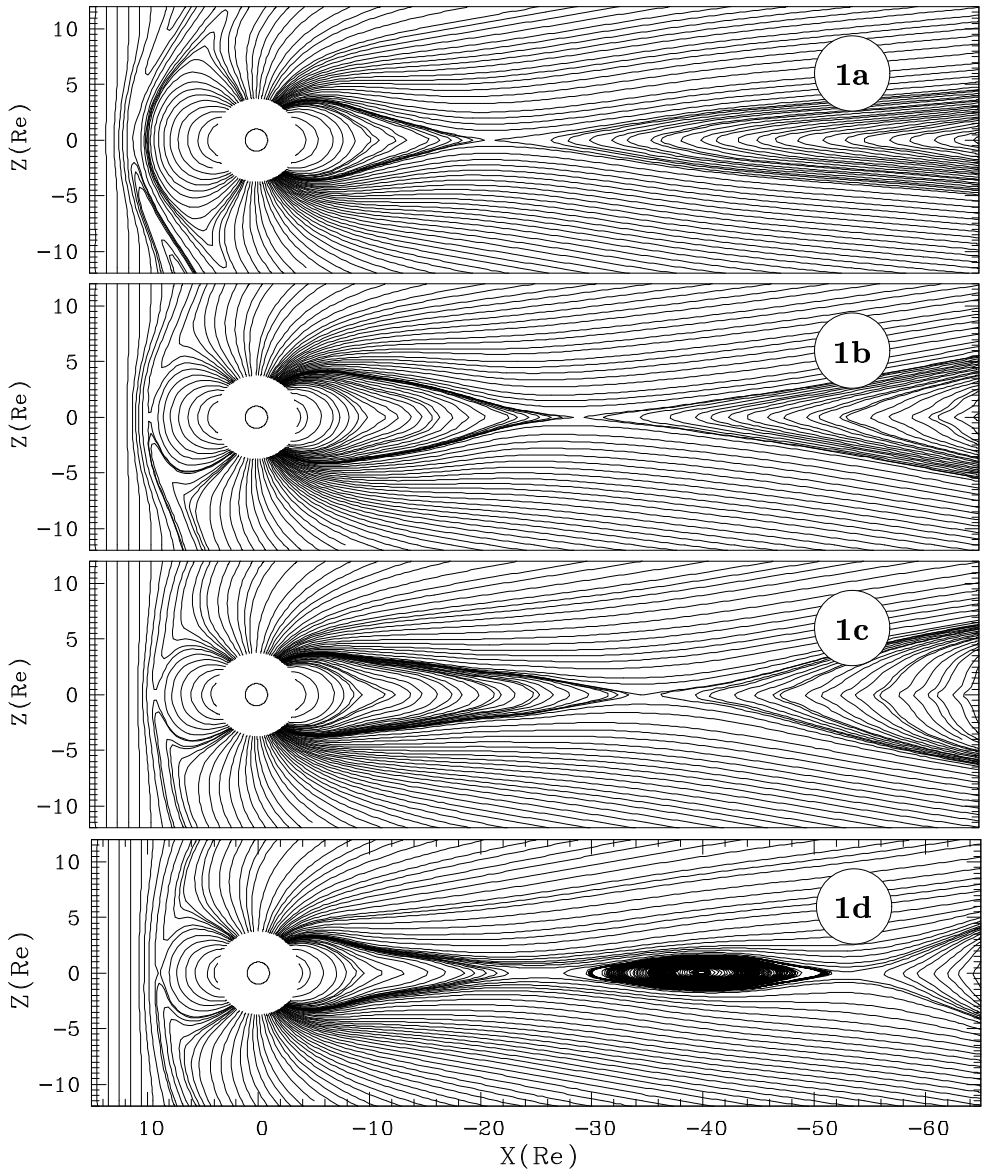

Figure 1. Time evolution of the magnetic field in the noon-midnight meridional plane for the reference run with self-consistent ionosphere and anomalous resistivity. The snapshots are taken at 125(1a), 135(1b), 145(1c), and 150(1d) minutes, respectively.

2.) *Self-consistent ionosphere but no anomalous resistivity*

Figs. 2a and 2b show the time evolution in the simulation run that does not include anomalous resistivity, i.e., with α = 0. These two figures correspond to the figures 1a and 1d of the reference run. The other two snapshots are not shown here because they are almost identical with figure 2b. In this simulation run, dayside and tail reconnection occurs because of the residual numerical resistivity.

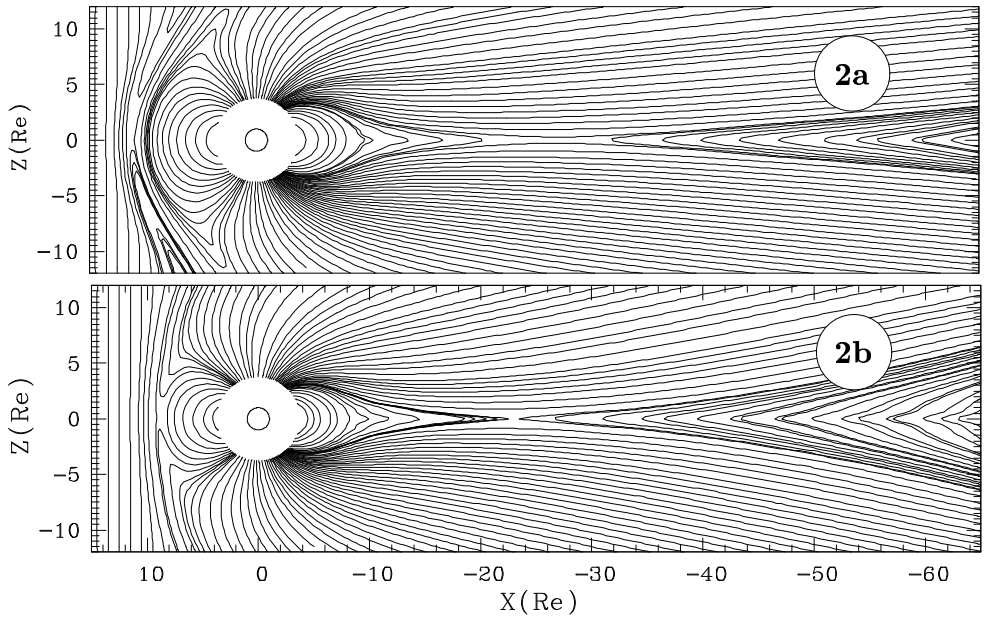

Figure 2. Time evolution of the magnetic field in the noon-midnight meridional plane for the run without anomalous resistivity. The snapshots are taken at 125(2a), and 150(2b) minutes, respectively.

The reconnection rate in the tail is lower than in the reference run, and as a result less flux is carried earthward. Therefore, the size of the closed field line region remains unchanged in time. In fact, there seems to be a perfect balance between the dayside reconnection rate, the nightside reconnection rate, and the transport rate by which flux is convecting back from the nightside to the dayside. This "steady convection" configuration does not change, even when the simulation is continued for much longer times. Although steady convection episodes are known to occur during times of southward IMF, they are usually initiated by a substorm [21]. Because this is not the case in the present simulation, we believe that the tail dynamics of this simulation are not realistic.

3.) *Anomalous resistivity and higher ionospheric conductance*

In this simulation run we have kept the anomalous resistivity as that used in the reference run, but have set the ionospheric Hall and Pedersen conductance Σ_H and Σ_P to a constant value of 50 Siemens. This value is considerably higher than normally observed in the ionosphere. Typical values range from some 10^{-1} to 20 Siemens [22]. Also, because there are no gradients in the Hall conductance, ionospheric Hall currents vanish. The results of this simulation run are shown in Fig. 3a-3c. The simulation run behaves initially (Fig. 3a) like the reference run (Fig. 1a). However, at later times (Fig. 3b and 3c) the effect of the increased conductance becomes evident. Because of the high conductance, field lines are effectively tied in the ionosphere. Ionospheric, and therefore magnetospheric con-

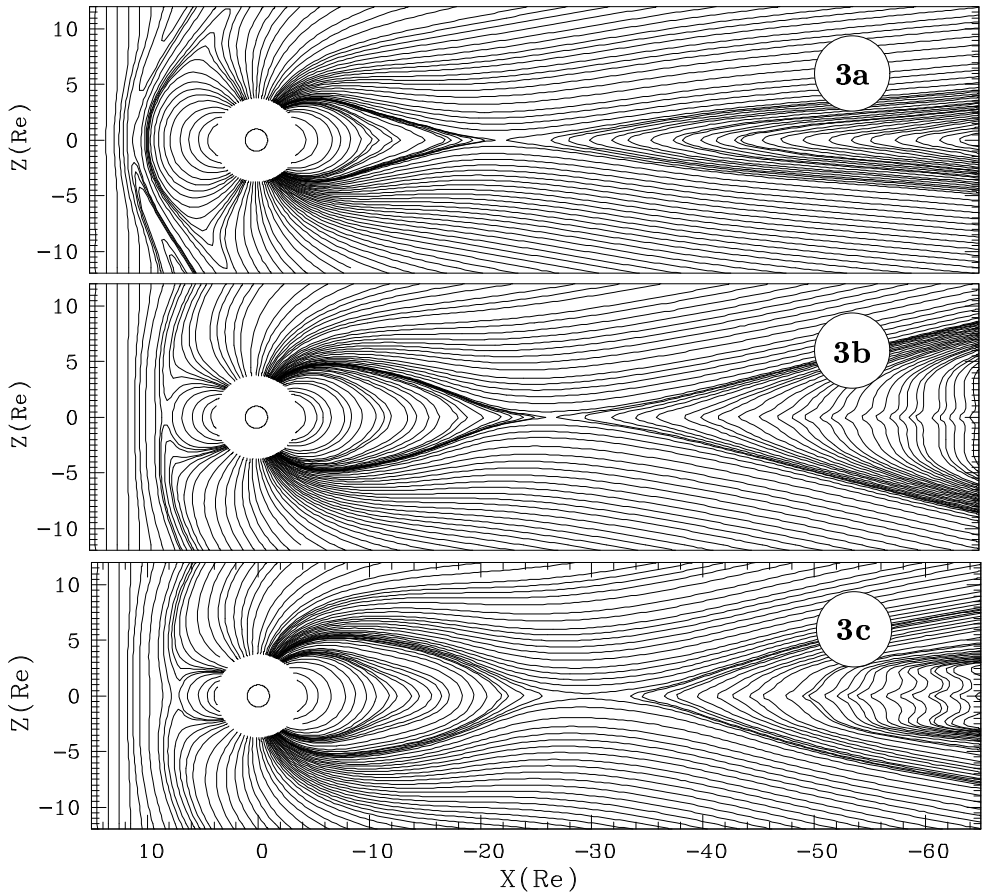

Figure 3. Time evolution of the magnetic field in the noon-midnight meridional plane for the run with increased ionospheric Hall and Pedersen conductance. The snapshots are taken at 125(3a), 150(3b), and 180(3b) minutes, respectively.

vection cannot proceed. The magnetospheric (closed) field on the dayside is not being replenished, leading to rapid earthward movement of the dayside magnetopause. Similarly, closed magnetic flux that is created by nightside reconnection piles up and pushes the neutral line tailward. Because of this flux imbalance, the whole auroral oval shifts sunward (not shown here). There are no signs of an instability occurring in the tail. Eventually (after a few hours), the system will achieve a convection balance. However, many of the parameters, for example the region 1 Birkeland currents, reach unrealistic values.

IV. DISCUSSION

We have used our global MHD model to study the effects of small scale processes and their parameterization on the dynamics of the magnetosphere.

First, we compare the reference run with the simulation run in which the anomalous resistivity term was switched off. These two simulations show

drastically different behaviours of the tail. By and large, the reference run, i.e., including a model of anomalous resistivity, shows a tail evolution that is in fairly close agreement with what is typically observed during substorms. In particular, the ejection of plasmoids (or flux ropes) in connection with substorms seems to be a well established feature [20]. However, we should caution against a direct comparison of any details in the reference run with substorm observations or with phenomenological substorm models. Substorms appear in a great variety of sizes and forms which seem to be very sensitive to the IMF history and solar wind parameters (see for example [23]). In this simulation run we used solar wind parameters that are rather unlikely to occur, in particular the IMF had no B_y component. Detailed comparisons between data and the model require that the model is run with measured solar wind data as input.

Three conclusion can be drawn from the comparison of these two simulation runs.

First, it seems that the numerical resistivity in our model is lower than the physical resistivity, at least in those regions of the magnetosphere and during those times where the physical resistivity reaches its highest values. This gives us more confidence in our simulation results, because numerical effects are apparently becoming less significant than the physical ones.

Second, the comparison of the two simulations provides evidence that some sort of anomalous resistivity[1] must be present for substorms to occur. Of course, the global simulations give no clue as to what the physical nature of the anomalous resistivity is. Although based on local theoretical studies [24-26], our resistivity model remains mostly phenomenological until now. Measurements of resistivity are very difficult [27], and therefore our understanding of the kinetic processes that lead to a violation of the ideal Ohm's Law is limited. We hope that forthcoming multipoint space missions will yield new data that lead to a better understanding of these kinetic processes and help us to improve our model.

Third, the comparison shows how critically the dynamics of the magnetosphere depends on a local, small scale process like anomalous resistivity. Although the MHD equations were altered only in a very small region (as compared to the size of the magnetosphere), this change leads to processes that affect the magnetospheric topology in a wide region and in a very short time.

The comparison of the reference run with the run with increased ionospheric conductance shows how tightly the magnetospheric dynamics are connected to the ionosphere. One implication is, of course, that it is important to model the ionosphere and its coupling with the magnetosphere in a proper fashion in order to address the magnetospheric dynamics correctly. Fortunately, much more observational data are avalaible for the ionosphere than for the tail. We compared

[1] The term 'anomalous resistivity' is used in a broad sense here and is meant to include all processes that are capable of violating the ideal Ohm's Law $\underline{\mathbf{E}} + \underline{\mathbf{v}} \times \underline{\mathbf{B}} = 0$.

the conductances in our model with statistical observations [22,28] and find in general a good agreement with these observations. Thus, although our ionospheric model is rather crude and built on simple approximations and empirical models, it seems to serve fairly well as a first order approximation.

The comparison of these two runs also shows that the evolution of reconnection processes in the tail is not only controlled by local parameters, i.e., anomalous resistivity, but by the ionospheric boundary conditions as well. Although we changed the boundary conditions rather drastically in the latter simulation run, the formation of a second (near-earth) neutral line and the formation of a plasmoid/flux rope was completely inhibited, despite the presence of anomalous resistivity.

The three simulations runs discussed here do not allow us to assess which of the two proceesses, i.e., anomalous resistivity or ionospheric conductance, is more important in controlling tail dynamics. Certainly, more simulations with varying parameters and careful comparisons with observations are necessary to gain better insight into these processes and their intricate relation. However, it is clear from the above results that any successful substorm model would necessarily include both of these processes.

In conclusion, our results show that the global configuration and dynamics of the magnetosphere depends critically on localized, small scale processes, and that carefully choosen parameterizations of these small scale processes are an important ingredient of any global magnetosphere model.

ACKNOWLEDGEMENTS

This research is supported by NASA-ISTP grant NAGW-1100 at UCLA. Computations were carried out on the Intel Paragon at the San Diego Supercomputer Center.

REFERENCES

[1] J. N. Leboeuf, T. Tajima, C. F. Kennel, and J. M. Dawson, Geophys. Res. Lett., **5**, 609 (1978).

[2] S. H. Brecht, J. G. Lyon, J. A. Fedder, and K. Hain, J. Geophys. Res., **87**, 6098 (1982).

[3] T. Ogino, J. Geophys. Res., **91**, 6791 (1986).

[4] J. A. Fedder, and J. G. Lyon, Geophys. Res. Lett., **14**, 880 (1987).

[5] J. Raeder, R. J. Walker, and M. Ashour-Abdalla, Geophys. Res. Lett., **22**, 349 (1995).

[6] L. A. Frank, M. Ashour-Abdalla, J. Berchem, J. Raeder, W. R. Paterson, S. Kokubun, T. Yamamoto, A. J. Lazarus, R. P. Lepping, F. V. Coroniti, D. H. Fairfield, and K. L. Ackerson, J. Geophys. Res., **100**, 19177 (1995).

[7] G. A. Sod, *Numerical Methods in Fluid Dynamics* (Cambridge University Press, Cambridge, 1985).

[8] G. A. Sod, J. Comp. Phys., **27**, 1 (1978).
[9] C. Hirsch, *Numerical Computation of Internal and External Flows, Volume II* (Wiley, New York, 1990).
[10] M. Hoshino, J. Geophys. Res., **96**, 11555 (1991).
[11] T. Sato and T. Hayashi, Phys. Fluids, **22**, 1189 (1979).
[12] A. Harten and G. Zwas, J. Comp. Phys., **9**, 568 (1972).
[13] C. R. Evans and J. F. Hawley, Ap. J., **332**, 659 (1988).
[14] T. Kamide and S. Matsushita, J. Geophys. Res., **84**, 4083 (1979).
[15] J. Moen and A. Brekke, Geophys. Res. Lett., **20**, 971 (1993).
[16] S. Knight, Planet. Space Sci., **21**, 741 (1972).
[17] L. R. Lyons, D. S. Evans, and R. Lundin, J. Geophys. Res., **84**, 457 (1979).
[18] C. F. Kennel and H. E. Petschek, J. Geophys. Res., **71**, 1 (1966).
[19] R. M. Robinson, R. R. Vondrak, K. Miller, T. Dabbs, and D. Hardy, J. Geophys. Res., **92**, 2565 (1987).
[20] M. B. Moldwin and W. J. Hughes, J. Geophys. Res., **98**, 81 (1993).
[21] A. Yahnin, M. V. Malkov, V. A. Sergeev, R. J. Pellinen, O. Aulamo, S. Vennerstrom, E. Friis-Christensen, K. Lassen, C. Danielsen, J. D. Craven, C. Deehr, and L. A. Frank, J. Geophys. Res., **99**, 4039 (1994).
[22] R. W. Spiro, P. H. Reiff, and L. J. Maher, Jr., J. Geophys. Res., **87**, 8215 (1982).
[23] R. D. Elphinstone, D. J. Hearn, L. L. Cogger, J. S. Murphree, H. Singer, V. Sergeev, K. Mursula, D. M. Klumpar, G. D. Reeves, M. Johnson, S. Ohtani, T. A. Potemra, I. Sandahl, E. Nielsen, M. Persson, H. Opgenoorth, P. T. Newell, and Y. I. Feldstein, J. Geophys. Res., **100**, 7937 (1995).
[24] J. D. Huba, N. T. Gladd, and J. F. Drake, J. Geophys. Res., **86**, 5881 (1981).
[25] S. P. Gary, Phys. Fluids, **23**, 1193 (1980).
[26] A. T. Y. Lui, P. H. Yoon, and C. L. Chang, J. Geophys. Res., **98**, 153 (1993).
[27] C. A. Cattell and F. S. Mozer, in Magnetotail Physics, A. T. Y. Lui, ed., (John Hopkins University Press, Baltimore and London, 1987), p. 119.
[28] D. A. Hardy, M. S. Gussenhoven, R. Raistrick, and W. J. McNeil, J. Geophys. Res., **92**, 12275 (1987).